TUTORIAL | JANUARY 15 2026

Parameter-drift models for plasma physics

Special Collection: Introductory Tutorials in Plasma Physics

Gabriel C. Grime ; Iberê L. Caldas ; Philip J. Morrison

Phys. Plasmas 33, 010901 (2026)
https://doi.org/10.1063/5.0307494
CHORUS

Physics of Plasmas TUTORIAL pubs.aip.org/aip/pop

Parameter-drift models for plasma physics

Cite as: Phys. Plasmas **33**, 010901 (2026); doi: 10.1063/5.0307494
Submitted: 16 October 2025 · Accepted: 13 December 2025 ·
Published Online: 15 January 2026

Gabriel C. Grime,[1,2,a] Iberê L. Caldas,[1] and Philip J. Morrison[2]

AFFILIATIONS

[1]Institute of Physics, University of São Paulo, São Paulo 05508-090, Brazil
[2]Department of Physics and Institute for Fusion Studies, The University of Texas at Austin, Austin, Texas 78712, USA

Note: This paper is part of the Special Topic on Introductory Tutorials in Plasma Physics.
[a]**Author to whom correspondence should be addressed:** gabrielgrime@usp.br

ABSTRACT

Fully self-consistent models have driven major advances in plasma simulation, supported by a rapid growth in computational performance. However, their high computational and energy costs highlight the need for accurate, reduced models. One promising approach is parameter-drift modeling, in which selected parameters evolve according to prescribed time laws rather than being coupled self-consistently to all other model variables. In this tutorial, we introduce key concepts in parameter-drift dynamical models and explore their applications in plasma physics. Using a familiar test-particle guiding-center model, we present the main analysis tools of the parameter-drift literature, namely, the ensemble approach, and discuss their advantages and limitations in Hamiltonian systems. Furthermore, we describe the dynamics of the model with traditional tools from dynamical systems theory, e.g., the Lyapunov exponent. In summary, we highlight the potential of parameter-drift models as reduced but insightful representations of time-dependent plasma dynamics. Although they cannot replace large-scale simulations with full bidirectional coupling between particles and fields, parameter-drift dynamical models offer an efficient framework for developing and testing fundamental aspects of time-dependent scenarios using reduced models.

I. INTRODUCTION

Advances in plasma simulations have been achieved by innovations in both analytical and computational methods.[1] As a rule, plasma models have become substantially more complex and sophisticated over the last decades. Progress has been stimulated by the cost reduction and rapid growth in computational performance in the last 50 years.[2] However, technological drive has somewhat been abated because computational performance is no longer progressing at a fixed cost and computational power consumption is quickly increasing.[3] Given this scenario, the evolution in computational methods can no longer be supported by the increasing complexity of the models; therefore, simplified and insightful models in plasma physics describing the main features of the considered models are needed.

The most performance-consuming source of plasma physics simulations is the desire to compute the fully self-consistent coupling between fields and particles. Kinetic and fluid models typically evolve a large number of variables simultaneously and independently, resulting in time-consuming and resource-intensive computations.[4,5] As an alternative, one can adopt parameter-drift models, in which selected parameters evolve according to predefined time-dependent evolution laws rather than being computed self-consistently from the internal dynamics of the model.[6] Within this framework, we attempt to reduce computational cost while still capturing essential aspects of the slow time evolution of key plasma quantities.

In this context, low-dimensional models offer a valuable framework for exploring the qualitative behavior of such systems. Despite their simplicity, these models can capture essential features that also govern more sophisticated models.[7–9] They provide analytical tractability, computational efficiency, and a clear setting in which to develop and extensively test theoretical models at low cost. Particularly in fluid mechanics and plasma physics, low-dimensional models have long served as idealized platforms for investigating fundamental transport processes[10–16] and guiding-center dynamics.[17–21] Moreover, their utility extends beyond plasma applications, offering insight into general features of systems governed by slowly varying or externally prescribed parameters.

Concerning dissipative low-dimensional systems, slow parameter-drift models have shown insightful results in the understanding of climate change dynamics subjected to time-dependent parameters such as greenhouse gas and aerosol emissions.[22–24] Recently, an ensemble approach for dealing with climate dynamics was proposed, called climate parallel realizations.[24] In this framework, the time evolution of

the climate is characterized by an ensemble of possible states, rather than the past time series of a given orbit in the ensemble.[25] In dynamical systems language, chaotic attractors constitute such ensembles, and the time evolution of the attractor dictates the time evolution of all possible parallel climate realizations.

Only recently has the framework of parameter-drift models been used for conservative and Hamiltonian systems.[6,26] Based on the ideas of parallel climate evolution, authors have employed the ensemble approach to describe time-dependent Hamiltonian system dynamics to gain insights into the corresponding physical models for magnetically confined fusion[27] and astrophysics.[28] However, the primary analysis tool used in the parameter-drift literature, the ensemble approach, was developed for dissipative systems and has intrinsic limitations when applied to conservative Hamiltonian systems, which lack attractors and feature a complex mix of regular and chaotic orbits. Therefore, the very concept of a representative ensemble of trajectories is conceptually hard to define and difficult to manipulate.

The purpose of this tutorial is to introduce the key concepts of parameter-drift models, emphasizing their significance and applicability in plasma physics modeling. Fundamental concepts and tools used in parameter-drift systems are presented in an accessible language for the plasma community, utilizing the parameter-drift version of a familiar guiding-center model for test particle orbits.[19]

The literature on parameter-drift models is based on the ensemble approach. Consequently, its main tools focus on ensemble-averaging indicators, such as the ensemble-average pairwise distance (EAPD) and the corresponding ensemble-average Lyapunov exponent (EALE).[29] We will address these tools, highlighting their advantages and limitations. We emphasize the constraints of the ensemble-averaging approach and its subsequent indicators by comparing them with the standard Lyapunov exponent, an orbit-wise quantity. This indicator requires a time-independent system; therefore, we demonstrate how to embed any parameter-drift Hamiltonian system into an extended phase space, eliminating explicit time dependence. As a result, the dynamics in the extended phase space preserve the original phase space structure but shed light onto important phenomena such as Arnold diffusion and the Arnold web.[30]

The tutorial begins in Sec. II with an in-depth look at the Hamiltonian test-particle guiding-center model, which will serve as an example throughout the paper. Section III starts with the definition of parameter-drift models and explains how such time-dependent dynamical systems differ from time-independent ones. We establish a parameter-drift version of the chosen example system in Sec. III A, demonstrating the consequences of including parameter drift in a previously time-independent system. The ensemble-average approach is presented in Sec. III B, along with its limitations. In Sec. IV, we detail the general procedure for converting a parameter-drift Hamiltonian system into a time-independent one, again using our example model. In the same section, we compare the results of the standard Lyapunov exponent of orbits in the new time-independent system with the ensemble-average Lyapunov exponent. Conclusions and final perspectives are provided in Sec. V.

II. TEST PARTICLE MAP

As noted above, in this tutorial we will utilize a low-dimensional Hamiltonian model to illustrate the principles and techniques presented here, due to its straightforward nature. However, these techniques can also be applied to more complex models. Although the drift wave test particle model involves certain oversimplifications, it effectively captures crucial aspects of edge $\mathbf{E}\times\mathbf{B}$ transport. In this model, the guiding-center equations of motion for a test particle are provided as follows:

$$\frac{\mathrm{d}\mathbf{x}}{\mathrm{d}t} = v_{\parallel}\frac{\mathbf{B}}{B} + \frac{\mathbf{E}\times\mathbf{B}}{B^2}, \tag{1}$$

where $\mathbf{x} = (r, \theta, \varphi)$ represents toroidal coordinates on a rectified torus, with $z = R\varphi$ and R denoting the major radius.[19] The electric field consists of a radial mean component $\overline{E}_r$ combined with a fluctuating component $\tilde{\mathbf{E}} = -\nabla\tilde{\phi}$ originating from the drift wave spectrum

$$\tilde{\phi}(\mathbf{x}, t) = \sum_{m=-\infty}^{\infty} \phi_m \cos(M\theta - L\varphi - m\omega t). \tag{2}$$

In components, Eq. (1) gives

$$\frac{\mathrm{d}r}{\mathrm{d}t} = -\frac{1}{rB}\frac{\partial\tilde{\phi}}{\partial\theta}, \tag{3a}$$

$$\frac{\mathrm{d}\theta}{\mathrm{d}t} = \frac{v_{\parallel}}{r}\frac{B_\theta}{B} - \frac{\overline{E}_r}{rB}, \tag{3b}$$

$$\frac{\mathrm{d}\varphi}{\mathrm{d}t} = \frac{v_{\parallel}}{R}. \tag{3c}$$

Assuming an infinite spectrum of modes with equal amplitude, $\phi_m = \phi$, one can derive a map from the differential equations (3) by applying the sifting property of the Dirac delta function.[19,31] The resulting map is given by

$$I_{n+1} = I_n + \frac{4\pi M\phi}{\omega a^2 B_\varphi}\sin(M\theta_n - L\varphi_n), \tag{4a}$$

$$\theta_{n+1} = \theta_n + \frac{2\pi}{R\omega}\frac{v_{\parallel}}{q(I_{n+1})} - \frac{1}{a\omega B_\varphi}\frac{\overline{E}_r(I_{n+1})}{\sqrt{I_{n+1}}}, \tag{4b}$$

$$\varphi_{n+1} = \varphi_n + \frac{2\pi}{R\omega}v_{\parallel}. \tag{4c}$$

Here, a denotes the minor radius, $q = rB_\varphi/(RB_\theta)$ is the safety factor, and $I = (r/a)^2$. The map defined by Eqs. (4) has three variables but can be interpreted as a four-dimensional Hamiltonian system. The momentum conjugate to the φ is a constant; therefore, φ is an ignorable coordinate.

In order to take into account the dynamics of φ without increasing the dimensionality, we can also define a new coordinate, $\chi := M\theta - L\varphi$ and write the map in terms of it, yielding

$$I_{n+1} = I_n + \frac{4\pi M}{a^2\omega}\frac{\phi}{B_\varphi}\sin(\chi_n), \tag{5a}$$

$$\chi_{n+1} = \chi_n + \frac{2\pi v_{\parallel}}{\omega R}\frac{[M - Lq(I_{n+1})]}{q(I_{n+1})} - \frac{M}{\omega a}\frac{\overline{E}_r(I_{n+1})}{B_\varphi\sqrt{I_{n+1}}}. \tag{5b}$$

The safety factor q and the radial electric field $\overline{E}_r$ are functions of the radius r, or equivalently, of the action I. Depending on the chosen profiles, the map exhibits different behaviors, governed by its *twist function*

$$\tau(I) = \frac{2\pi v_{\parallel}}{\omega R}\frac{[M - Lq(I)]}{q(I)} - \frac{M}{\omega}\frac{\overline{E}_r(I)}{B_\varphi\sqrt{I}}, \tag{6}$$

which gives the frequency, or equivalently, the period, of each orbit in the integrable limit, i.e., when $\phi = 0$. The meaning of the twist function in Hamiltonian dynamical systems is somewhat elaborate. Fortunately, it has a direct correspondence with a well-known concept in magnetic fusion: the rotational transform in tokamaks. In this analogy, the twist function can be interpreted as measuring the rotational transform, that is, the number of poloidal transits per toroidal transit, of a trajectory in phase space. Since the Hamiltonian phase space in action–angle variables has the topology of a torus, the twist function essentially quantifies this winding property. Furthermore, as for the rotational transform in tokamaks, the twist function profile is fundamental for transport properties in Hamiltonian systems, as we will see next.

Early research on rotating fluid experiments[10,32] showed that barriers to transport appear near the peak of zonal flows. Because the equations governing these experiments are to leading order equivalent to the Hasegawa–Mima equations that govern plasma drift waves, del-Castillo-Negrette and Morrison proposed at this time that the same would be true in the plasma zonal flow context and, moreover, that it was a general feature of systems where the twist function possesses extrema, so-called nontwist or shearless points. It was also proposed in the context of magnetic confinement devices that this should be the case for extrema of the rotational transform.[33] The reason for this is because near nontwist points, in general, in classes of systems, it is difficult for perturbations to generate adjacent large-scale resonances.[11,34,35] These ideas have appeared in many places over the years, e.g., in Refs. 36 and 37, where they were seen to be consistent with experimental observations in two other devices.

Indeed, in advanced tokamak scenarios, internal transport barriers are now associated with reversed shear q profiles,[38] while edge transport barriers are associated with steep wells[39] or hills[40] on $\overline{E}_r$ profiles at the plasma edge. Both scenarios exhibit reduced transport coefficients near the extrema of these profiles, characterizing the formation of particle transport barriers.

In the context of our Hamiltonian model, using nonmonotonic profiles of safety factor and radial electric field, extremum points (maxima or minima) in the twist function appear, i.e., (I^*, χ^*) points in phase space at which

$$\left.\frac{\mathrm{d}\tau}{\mathrm{d}I}\right|_{(I^*,\chi^*)} = 0\,; \tag{7}$$

these are the nontwist or shearless points proposed by del-Castillo-Negrette and Morrison, which generate shearless orbits: special tori that are characteristically resistant to perturbations.

In order to produce both internal and edge transport barriers, safety factor and electric field profiles are chosen as follows:

$$q(\rho) = q_{\mathrm{m}} + \gamma(\rho - \rho_q)^2, \tag{8a}$$

$$\overline{E}_r(\rho) = -\frac{\rho A}{1 + \eta\left(\rho^2 - \rho_{\mathrm{E}}^2\right)^2}. \tag{8b}$$

Here, ρ is the normalized radial coordinate, and

$$\gamma = (q_0 - q_{\mathrm{m}})/\rho_q. \tag{9}$$

All parameter values, listed in Table I, assumed in this work correspond to those reported for the observed TCABR tokamak discharges.[16,41] The radial profiles of the safety factor and the electric field are shown in Fig. 1(a).

TABLE I. Parameters used throughout the paper.

Parameter	SI	Normalized
M	15	15
L	6	6
B_φ	1 T	1
ω	6×10^4 Hz	6
$v_{\|\|}$	3 km/s	1.5
q_0	3	3
q_{m}	2	2
ρ_E	0.95	0.95
ρ_q	0.4	0.4
A	2 kV/m	1.0
η	80	80

These profiles give rise to the twist function shown in Fig. 1(b), which exhibits three shearless points: $I_1 \approx 0.2$, $I_2 \approx 0.9$, and $I_3 \approx 0.7$. The first two correspond to the minimum and maximum of $q(I)$ and

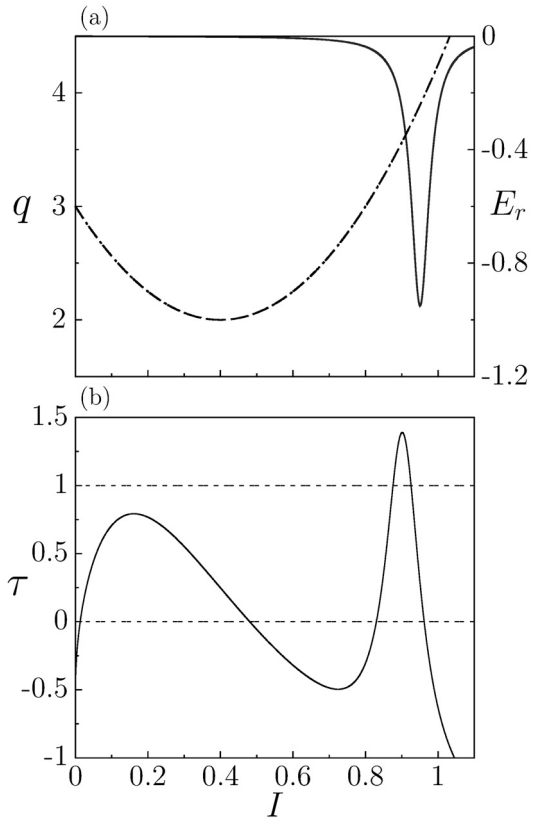

FIG. 1. Radial profiles of (a) the safety factor q (dashed lines) and equilibrium electric field $\overline{E}_r$ (filled line) and (b) the corresponding twist function τ.

$\overline{E}_r(I)$, respectively. The third shearless point, located between them, emerges from the combined influence of the two profiles.

Typical phase space plots using the profiles of Fig. 1 are shown in Fig. 2, presenting both regular (resonances and tori) and chaotic orbits. In phase space, transport takes place by chaotic orbits, which occupy a significant fraction of phase space. With the increase in perturbation, the drift wave amplitude ϕ in our model, chaos spreads through phase space, destroying resonances and tori. In the transition between Figs. 2(a) and 2(b), the blue and green shearless tori are broken in the process of chaos spreading. Among regular orbits, shearless tori play a key role in phase space transport. Due to their shearless nature, they are robust against perturbations. For example, the green shearless torus in Fig. 2(a), corresponding to the edge transport barrier, is one of the last surviving tori and prevents radial chaotic transport in that region.

Moreover, even after the shearless torus breakup, remnants of the shearless torus still act as a partial transport barrier. Transport coefficients in the region are reduced, mostly influenced by hyperbolic manifolds crossing in the region.[42] The partial transport barrier strength is sensitively dependent on parameters.

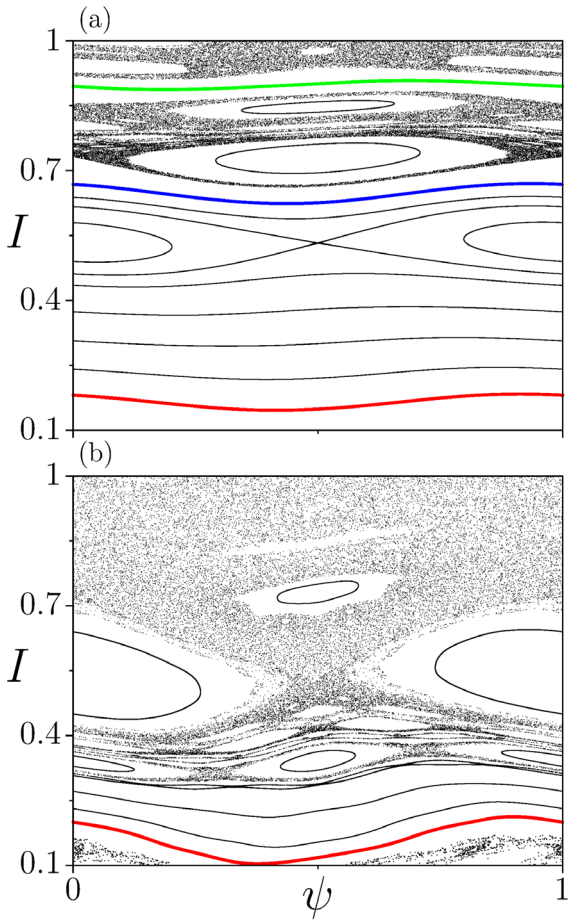

FIG. 2. Phase space. (a) $\phi = 0.6 \times 10^{-3}$ and (b) $\phi = 1.8 \times 10^{-3}$. The shearless orbits, in green, blue, and red, prevent chaotic transport. With the increase in perturbations, the edge transport barrier is broken.

In this section, we presented the drift wave test particle map for the guiding-center dynamics of test particles in plasmas subject to electrostatic perturbations present in edge turbulence. By using non-monotonic profiles consistent with advanced scenarios in tokamak discharges, the system shows regions in phase space with reduced transport coefficients, fundamentally due to the existence of shearless tori and their remnants.

III. SLOW PARAMETER-DRIFT MODELS

In plasma physics, as in many other fields, the relevant quantities are typically classified into two categories: dynamical variables and parameters. Dynamical variables refer to physical quantities that evolve over time, such as position and velocity. Parameters, on the other hand, are fixed quantities defined by the model.

However, plasma parameters such as electron temperature, plasma current, and instability amplitude are not constant in many plasma models. In such cases, these quantities must be treated as dynamical variables and solved self-consistently by the model, leading to computationally expensive simulations. Despite the high computational cost, the physical accuracy of the results strongly depends on the quality of the self-consistent formulation.

Ultimately, the distinction between variables and parameters is determined by the model itself. To reduce computational cost while still capturing essential aspects of the time evolution of key plasma quantities, one may instead prescribe a time evolution for selected slow-varying parameters. This leads to a parameter-drift model, in which some parameters evolve according to pre-established time evolution, rather than depending on the variables of the model.

In general terms, a parameter-drift model is a dynamical system defined by the class of equations

$$\dot{\mathbf{z}} = \mathbf{F}(\mathbf{z}, \boldsymbol{\mu}(t), t), \quad t_0 \le t \le t_{\max}, \tag{10}$$

where $\mathbf{z} \in D$ is the vector of dynamical variables in the phase space D, $\mathbf{F} : D \to D$ is a vector-valued function that governs the evolution of the dynamical variables, and $\boldsymbol{\mu}(t)$ denotes the set of time-dependent parameters. In the case of discrete-time systems, time takes on integer values $n = 0, 1, \ldots$, and the time evolution is described by a map

$$\mathbf{z}_{n+1} = \mathbf{M}(\mathbf{z}_n, \boldsymbol{\mu}_n), \quad n_0 \le n \le n_{\max}, \tag{11}$$

where $\boldsymbol{\mu}_n \equiv \boldsymbol{\mu}(n)$ is a function of discrete time n. These definitions can also be extended to models involving partial differential equations.

Since we are focusing on slow parameter drifting, the ordering of this drift must obey certain bounds. A rough estimate can be established by the ratio $R = |\mu'|/\mu_0$, which measures the parameter shift compared to its initial value. Considering $R \ll 1$, typically $R < 10^{-2}$, is sufficient for our purpose.

One can notice that Eqs. (10) and (11) define evolution rules with explicit time dependence, characterizing them as nonautonomous dynamical systems. In contrast to autonomous systems, whose evolution laws are time-independent, nonautonomous systems can exhibit richer dynamics.[22] Although many classic differential equations books treat nonautonomous systems,[43] in recent years a broad class of the dynamical systems literature in both mathematics and the physical sciences has concentrated on autonomous systems. However, interesting intrinsically nonautonomous phenomena, such as tipping points and hysteresis-like bifurcation processes, can be crucial in many nonautonomous drift parameter contexts.[44,45]

A. Parameter drift in plasma physics

Symplectic low-dimensional parameter-drift maps have recently attracted attention in the literature due to their connections with important phenomena in climate science.[6,26,29,46] However, only recently has their relevance to plasma physics been established.[27]

The plasma physics community is already using the parameter-drift approach on some equilibrium models. Recently, time-dependent solvers for the Grad–Shafranov equation have been proposed to account for the effects of slow dynamics, for example, caused by resistivity.[47,48] In these works, the Grad–Shafranov equation is self-consistently solved for the flux function with a constant electric resistivity that gives an inductive current. The authors claim that despite the finite lifetime of stationary solutions, one can get insightful results by coupling the equilibrium solution with slow time-dependent effects of resistive diffusion.[47]

In this tutorial, we will focus on our example model, given by Eqs. (5), while allowing parameters to vary over time. This leads to a time-dependent symplectic map. For instance, a linear drift in the perturbation amplitude $\phi = \phi(n) = \phi_0 + \phi' n$ yields

$$I_{n+1} = I_n + \frac{4\pi M}{a^2 \omega B_\varphi}(\phi_0 + \phi' n)\sin(\chi_n), \tag{12a}$$

$$\chi_{n+1} = \chi_n + \frac{2\pi \nu_{||}}{\omega R}\frac{[M - Lq(I_{n+1})]}{q(I_{n+1})} - \frac{M}{\omega a}\frac{\overline{E}_r(I_{n+1})}{B_\varphi \sqrt{I_{n+1}}}, \tag{12b}$$

where ϕ' is constant. Furthermore, any other parameter, e.g., the toroidal magnetic field and the radial profiles of equilibrium electric field and safety factor, may also be time-dependent within this model. Thus, depending on the physical aspect under consideration, parameters can be treated as either fixed or drifting.

The drift wave model can also be interpreted as a parameter-drift system by treating φ as a system parameter. Assuming a constant $\nu_{||}$ in Eqs. (4), the time evolution of the toroidal coordinate can be solved, yielding $\varphi(n) = \frac{2\pi\nu_{||}}{R\omega} n$. Therefore, the system reduces to a two-dimensional Hamiltonian map in the (I, θ) action–angle variables, with a time-dependent parameter $\varphi(n)$. In this context, ripples in the magnetic field lines can be added to the model considering $B_\varphi = B_\varphi(n)$, which is equivalent to a toroidal angle dependence in this framework.

Although substantial results have been established concerning paradigmatic low-dimensional dynamical systems with parameter drift,[6,26,29,49] the effects of parameter drifting in complex plasma models have not yet been studied. We argue that paradigmatic plasma systems keep a connection with their larger parent models, and the results obtained are useful for understanding the big picture.

As an example, consider a parameter-drift version of the standard nontwist map.[10,49] This is recovered in the local dynamics of Eqs. (12) by fixing to a parabolic safety factor profile

$$q(I) = q_{\mathrm{m}} + \frac{q''_{\mathrm{m}}}{2}(I - I_{\mathrm{m}})^2, \tag{13}$$

and disregarding the effect of the radial electric field. Then, upon Taylor expanding the equation for the angle and defining new variables,

$$x = \frac{\chi}{2\pi}, \quad y = \sqrt{\frac{M q''_{\mathrm{m}}}{2 q_{\mathrm{m}} \delta}}(I - I_{\mathrm{m}}),$$

we obtain the parameter-drift standard nontwist map

$$x_{n+1} = x_n + \alpha(1 - y_{n+1}^2), \tag{14a}$$

$$y_{n+1} = y_n - \beta(n)\sin(2\pi x_n), \tag{14b}$$

where

$$\alpha = \frac{\nu_{||}\delta}{R q_{\mathrm{m}} \omega}, \quad \beta(n) = \left(\frac{-2\pi M}{a^2 \omega}\right)\sqrt{\frac{2M q''_{\mathrm{m}}}{2 q_{\mathrm{m}} \delta}}\frac{\phi(n)}{B_\varphi}. \tag{14c}$$

Therefore, locally, the drift wave map around the minimum of the safety factor profile behaves as the time-dependent standard nontwist map,[49] with the perturbation parameter $\beta(n)$ varying over time.

Fundamentally, parameter-drift systems are nonautonomous. This results in time-dependent structures and components in phase space. However, parameter-drift maps do not possess the invariant structures as seen in two-dimensional autonomous maps, like the invariant tori shown in Fig. 2.

Depending on the regime of parameter variation, tori and chaotic seas can be interpreted as time-dependent structures within parameter-drift systems. For instance, Fig. 3 illustrates our example model with a linear time-dependent amplitude. We consider the so-called snapshot objects in phase space at various iteration times. An ensemble of trajectories is initialized in the frozen system ($\phi = 0$), similarly to the orbits shown in Fig. 2(a). These ensembles are then evolved under the parameter-drift system and plotted in phase space.

After a few iterations, structures in phase space become visible, but they are deformed due to the parameter variation. These variations tend to stretch and fold the snapshot objects, giving rise to fingerlike structures within the chaotic sea, particularly prominent around the main resonance inside the chaotic sea shown in Fig. 3(b). On nonresonant tori, the stretching and folding effects are even more pronounced. Eventually, the parameter drift causes the breakup of these tori through collisions with the chaotic saddle.[6] This occurs between Figs. 3(a) and 3(b) for the green torus and between Figs. 3(b) and 3(c) for the blue torus.

Before their breakup, shearless tori act as transport barriers in phase space, preventing the chaotic sea from spreading upward. The two chaotic regions above and below the green shearless torus only mix after its breakup, thereby creating a transport channel. A similar mechanism occurs with the blue torus.

In general, the evolution of such ensembles is related to the behavior of manifolds in the system, which, in time-varying systems, are referred to as time-dependent foliations.[26] Similar to invariant manifolds, stable and unstable foliations determine the repelling and attracting directions along which orbits travel through phase space. It is well established in the literature that hyperbolic manifolds give rise to Smale horseshoe sets. Specifically, in Hamiltonian systems, these horseshoes exhibit the characteristic fingerlike structures around resonances immersed in chaos.[42,50,51]

B. Ensemble-average pairwise distance

Traditionally, in dynamical systems, the chaoticity of an orbit is determined by its largest Lyapunov exponent. Fundamentally, this quantity characterizes the asymptotic rate of exponential divergence between nearby trajectories. Considering two-dimensional Hamiltonian maps, regular quasiperiodic orbits have a zero maximal Lyapunov exponent. In contrast, chaotic orbits have a positive Lyapunov exponent, which also serves as a measure of the intensity of chaos.

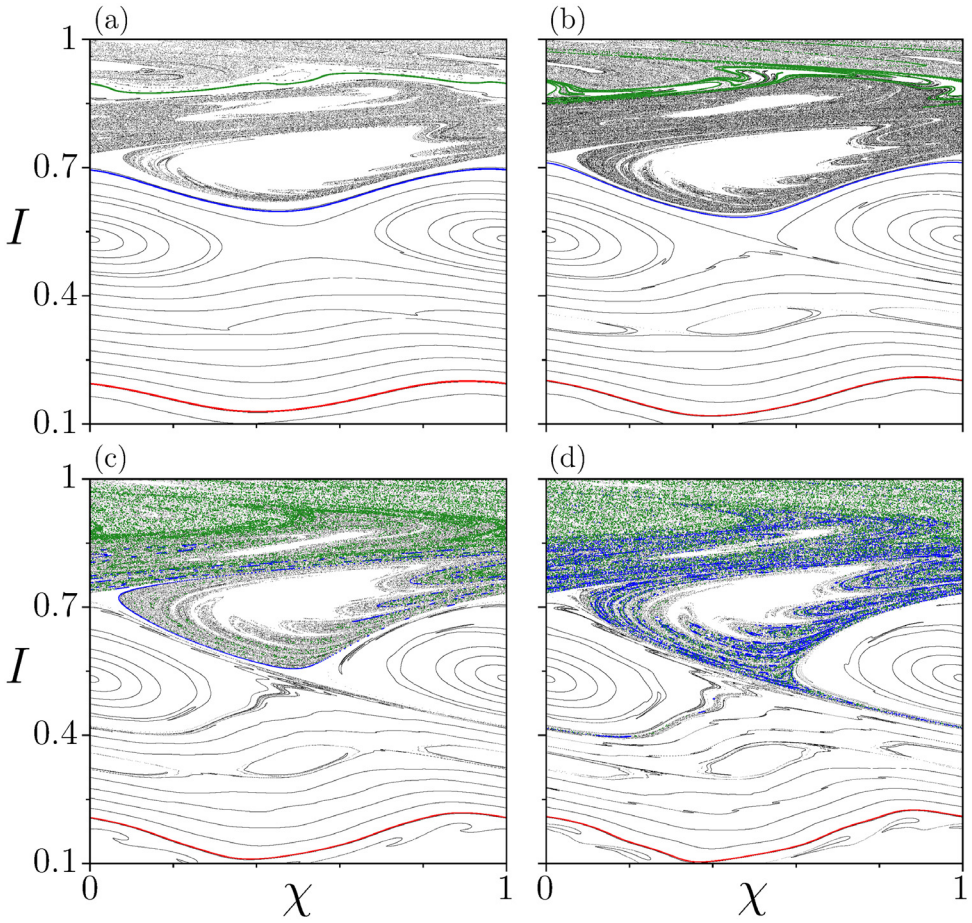

FIG. 3. Phase space snapshots of an ensemble of orbits evolved under a linear drift in the perturbation amplitude $\phi(n) = \phi_0 + \phi' n$ with values $\phi_0 = 0.6 \times 10^{-3}$, $\phi' = (\phi_{\max} - \phi_0)/n_{\max}$, $\phi_{\max} = 2.6 \times 10^{-3}$, $n_{\max} = 100$. All orbits are initialized on the "frozen" tori seen in Fig. 2(a). (a) $n = 30$, (b) $n = 45$, (c) $n = 60$, and (d) $n = 70$.

However, traditional dynamical system methods, such as the calculation of Lyapunov exponents, have not been applied to parameter-drift systems. Instead, the ensemble-average pairwise distance (EAPD) was proposed as a measure of the chaoticity of ensembles, that is, the time at which a given ensemble becomes chaotic, as well as to assess the strength of its chaotic behavior. Based on the exponential expansion of the ensemble of points, the EAPD is defined as

$$\rho(n) = \langle \ln d_n \rangle, \tag{15}$$

where the average $\langle \cdot \rangle$ is taken over an ensemble of trajectories, and d_n denotes the distance between neighboring trajectories within the ensemble at discrete time n.

We compute the EAPD for our parameter-dependent nontwist system. To this end, we initialize an ensemble with $N = 10^5$ initial conditions distributed along the shearless curve. For each initial condition, a nearby point within an ε-neighborhood is also selected. Both sets of initial conditions are evolved under the parameter-drift system. The initial separation is set as $d_0 = 10^{-10}$. At each time step n, the distance d_n between each orbit and its ε-neighbor is computed and then averaged over the ensemble.

The evolution of $\rho(n)$ is illustrated in Fig. 4 for the blue and green snapshot shearless tori. Initially, in both ensembles, the EAPD remains approximately constant at the numerical value corresponding to the initial separation set by the ε-neighborhood, $\rho(0) = \ln 10^{-10} \approx -23$. A transition then occurs from this initial plateau to a linear growth regime. Based on numerical estimates, we define a critical iteration value $n_c \approx 33$ for the green torus and $n_c \approx 55$ for the blue torus. This transition indicates the onset of exponential orbit separation, on average, within each ensemble. The slope, or the derivative, in the linear regime is interpreted as the instantaneous Lyapunov exponent associated with the ensemble. In this work, we refer to it as the ensemble-averaged Lyapunov exponent.

Eventually, the pairwise distance assumes the scale of phase space, and the EAPD saturates around zero. The presence of subregimes with different Lyapunov exponents is also possible. We found two such subregimes associated with the green torus. However, these can be difficult to define and detect numerically.[52]

The ensemble approach, by its averaging nature, provides only typical information about collections of trajectories and may obscure important dynamical features present within the ensemble. Authors argue that traditional Lyapunov exponents are inadequate

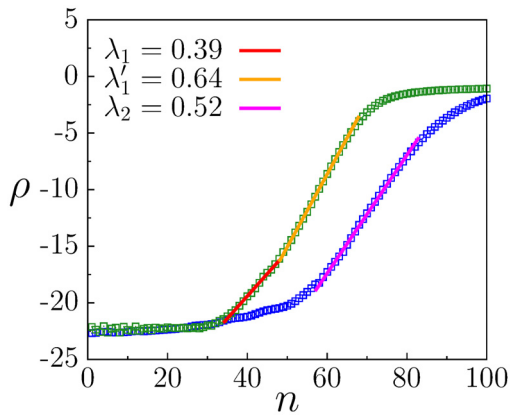

FIG. 4. Ensemble-average pairwise distance using the same parameters as in Fig. 3. Green (blue) points refer to the green (blue) shearless orbit. The corresponding ensemble-average Lyapunov exponents are indicated.

for parameter-drift systems, as their asymptotic definition is inconsistent with the finite-time windows inherent to these systems.[6] An alternative is to consider the finite-time Lyapunov exponent (FTLE), which captures the local divergence of trajectories over short, predefined time intervals. This yields a time-window-appropriate measure that also allows a per-orbit basis computation.

To compute traditional Lyapunov exponents in parameter-drift systems, it is often convenient to eliminate explicit time dependence. This can be achieved by treating time as an additional coordinate. However, care must be taken to preserve essential features of the system, such as its Hamiltonian structure. In Sec. IV, we present a proper formulation for removing explicit time dependence in Hamiltonian systems, enabling the computation of finite-time Lyapunov exponents for individual orbits.

IV. EXTENDED PHASE SPACE APPROACH

The ensembles in a Hamiltonian parameter-drift system deform (Fig. 3) as a result of explicit time dependence on the evolution equations of motion. This contrasts with time-independent Hamiltonian systems, whose chaotic seas, resonances, and irrational tori remain invariant under time evolution. Although both are Hamiltonian, the explicit time dependence imposed by the parameter evolution effectively increases the dimensionality of the phase space. In order to obtain an autonomous system with equivalent time evolution, one needs to extend the dimensionality of the system, considering time as a canonical coordinate. Formally, we embed the parameter-drift system into the extended phase space. For continuous Hamiltonian systems, the procedure is straightforward and well known.[30,53]

A. Time as a canonical variable

Consider a parameter-drift continuous Hamiltonian function given by

$$H(p,q,t) = H(p_1,\ldots,p_k,q_1,\ldots,q_k,\mu(t),t),$$

with canonical pairs of momentum and coordinate (p_i,q_i), $i=1,\ldots,k$. This defines a $2k$-dimensional phase space. We can embed this phase space into the so-called extended phase space by treating time t as an additional coordinate. Formally, we define a new canonical coordinate $q_{k+1} \equiv t$ and its conjugate momentum $p_{k+1} \equiv -H$. By defining the new Hamiltonian

$$\mathscr{H}(p,q) = p_{k+1} + H(p_1,\ldots,p_k,q_1,\ldots,q_k,\mu(q_{k+1}),q_{k+1}),$$

the resulting Hamiltonian system is autonomous, i.e., with no explicit time dependence. The system also preserves the original time evolution equations, and its $2(k+1)$-dimensional phase space keeps a Hamiltonian structure.

In our example parameter-drift system, Eq. (12), since it is a map, we do not have a Hamiltonian function generating the time evolution. Nevertheless, Hamiltonian maps are derived from an evolution rule involving the so-called generating function, which guarantees that the map preserves the geometric structure of the phase space, i.e., its symplecticity. Therefore, the time evolution $(\chi_n, I_n) \to (\chi_{n+1}, I_{n+1})$ is given by the generating function

$$F(I_{n+1},\chi_n;n) = \chi_n I_{n+1} + \frac{2\pi\nu}{\omega R}\left[M\int\frac{\mathrm{d}I_{n+1}}{q(I_{n+1})} - LI_{n+1}\right] - \frac{M}{a\omega B_\varphi}\int\frac{\bar{E}_r(I_{n+1})}{\sqrt{I_{n+1}}}\mathrm{d}I_{n+1} + \frac{2M\phi(n)}{a^2\omega B_\varphi}\cos(\chi_n). \quad (16)$$

One obtains the relations between the "old" (χ_n, I_n) and "new" (χ_{n+1}, I_{n+1}) coordinates according to

$$I_n = \frac{\partial F}{\partial \chi_n}, \quad \chi_{n+1} = \frac{\partial F}{\partial I_{n+1}}, \quad (17)$$

which recovers the parameter-drift Hamiltonian map under study. Note that the generating function itself has explicit time dependence. More about Hamiltonian maps and generating functions can be found in any Classical Mechanics textbook.[30,54,55]

In order to embed our two-dimensional map into the extended phase space, we propose a simple procedure based on the original system generating function.[56] Starting from the time-dependent generating function (16), we identify the iteration as the new coordinate x. Let (I,χ,y,x) be the canonical coordinates of a four-dimensional Hamiltonian map, where (I,y) are the canonical momenta conjugate to the coordinates (χ,x). The simplest generating function of the second kind is an extension of Eq. (16) given by

$$G(I_{n+1},\chi_n,y_{n+1},x_n) = F(I_{n+1},\chi_n;\phi(x_n)) + (x_n+1)y_{n+1}. \quad (18)$$

The first term corresponds to the generating function in Eq. (16), where the parameter ϕ is treated as a function of the coordinate x, which is interpreted as a time coordinate. The last term in Eq. (18) is based on the identity generating function but serves to increment x by one unit at each iteration. Hence, the coordinate x evolves analogously to time in our discrete map. This generating function implies the following relations:

$$I_n = \frac{\partial G}{\partial \chi_n} = \frac{\partial F}{\partial \chi_n},$$
$$\chi_{n+1} = \frac{\partial G}{\partial I_{n+1}} = \frac{\partial F}{\partial I_{n+1}},$$
$$y_n = \frac{\partial G}{\partial x_n} = \frac{\partial F}{\partial \phi}\frac{\mathrm{d}\phi}{\mathrm{d}x_n} + y_{n+1},$$
$$x_{n+1} = \frac{\partial G}{\partial y_{n+1}} = x_n + 1,$$

yielding the four-dimensional autonomous Hamiltonian map

$$I_{n+1} = I_n + \frac{4\pi M}{a^2 \omega B_\varphi}\phi(x_n)\sin(\chi), \tag{19a}$$

$$\chi_{n+1} = \chi_n + \frac{2\pi \nu_{||}}{\omega R}\frac{[M - Lq(I_{n+1})]}{q(I_{n+1})} - \frac{M}{\omega B_\varphi}\frac{\overline{E}_r(I_{n+1})}{\sqrt{I_{n+1}}}, \tag{19b}$$

$$y_{n+1} = y_n + \frac{2M}{a^2 \omega B_\varphi}\phi'(x_n)\cos(\chi_n), \tag{19c}$$

$$x_{n+1} = x_n + 1. \tag{19d}$$

Observe that the map of Eqs. (19) keeps the same drifting dynamics in (I, χ) plane, but now, the parameter ϕ drifts with the coordinate x instead of the time n. The new map also keeps the Hamiltonian structure, an important feature since our original parameter-drift map is also Hamiltonian. Nonetheless, its dimensionality is increased, which may complicate some numerical tasks but sheds light on important phenomena already observed in the system: the lack of invariant curves.

In Hamiltonian systems with more than two degrees of freedom, chaotic transport is strongly influenced by the so-called Arnold web: the intricate resonant network formed by the intersections of nonlinear resonance manifolds. Along this web, orbits transition between resonant layers, a mechanism known as Arnold diffusion. Unlike two-dimensional symplectic maps, where transport is strongly constrained by invariant tori, higher-dimensional systems possess no absolute barriers, and weak drift along resonances allows orbits to migrate across wide regions of phase space over long timescales. For a pedagogical introduction to the topic, see Ref. 57.

These ideas have been extensively developed in classical mechanics for near-integrable systems since the early work of Arnold.[58] Recent mathematical work has clarified how global transport can occur in multidimensional Hamiltonian systems through the interaction of resonances, the geometry of normally hyperbolic invariant manifolds (NHIMs), and the role of scattering maps.[59–63] In plasma physics, Arnold diffusion has been rigorously demonstrated for charged particles in ABC magnetic fields.[64] Its relevance for adiabatic invariant breakdown and toroidal confinement has been emphasized in studies of time-dependent magnetic configurations.[64,65]

B. Lyapunov exponent approach

As a general rule, the ensemble-average pairwise distance and its associated growth rate are statistical measures of the exponential separation of orbits, but they do not represent true Lyapunov exponents—even in the finite-time regime. Due to its averaging nature, the ensemble average can obscure relevant subpopulations exhibiting behavior that deviates from the mean, as we will show.

Fortunately, by embedding the parameter-drift system (12) into the extended phase space, we can compute the Lyapunov exponent of individual orbits in the autonomous system (19) using traditional and broadly tested algorithms.[66] Furthermore, we can visualize snapshots of each ensemble and track the time evolution of the finite-time Lyapunov exponent (FTLE) of each orbit (see Fig. 5). Since time acts as a coordinate in the extended phase space, snapshots correspond to stroboscopic maps.

In this work, we use the numerical method described in Ref. 66 to compute the full Lyapunov spectrum of individual orbits. This method is based on the Jacobian matrix and employs the Gram–Schmidt orthonormalization procedure to track the expansion and contraction rates along stable and unstable directions.

The time evolution of a blue shearless torus is depicted in Fig. 5, together with the largest FTLE of each orbit calculated for different times n, represented by the color bar. Initially, the torus ensemble deforms without losing its circular topology [Fig. 5(a)] until $n \approx 60$ when a population of orbits starts to stretch and fold [Fig. 5(b)]. Although this population begins to stretch and fold into the chaotic sea, a noticeable population of the ensemble remains regular [Fig. 5(c)].

The disparity of behaviors in the same ensemble is also reflected in the differences in the FTLE. Orbits with regular behavior tend to have small FTLE, especially in the initial iteration. Additionally, no single orbit in the ensemble shows an FTLE of 0.52, the value provided by the ensemble-average Lyapunov exponent (EALE). In summary, the EALE for this blue torus (Fig. 4) is therefore not representative of any specific orbit behavior but is rather a statistical mean that hides this rich dynamical complexity.

Since our parameter drift is strictly increasing, eventually all orbits tend to become fully chaotic, as shown in Fig. 5(d). Nevertheless, even among chaotic orbits, there is a substantial difference in the FTLE of orbits in the ensemble.

Shearless transport barriers also play a central role in this context. Notably, the chaotic region initially expands into the upper portion of the phase space. Only after a transient, the ensemble initialized on the shearless curve begins to extend into the region below it [Fig. 5(d)].

The reason why, even within the same ensemble, populations of orbits exhibit markedly different finite-time evolutions is investigated by analyzing the Lagrangian Coherent Structures (LCS) in phase space.[67–69] By computing the finite-time Lyapunov exponent on a grid of initial conditions in the (χ, I) plane, distinct coherent structures with varying FTLE values emerge, as shown in Fig. 6. Note that the procedure in Fig. 6 differs from that in Fig. 5. Instead of displaying snapshots and FTLE values at different iterations n, Fig. 6 presents the FTLE computed for a grid of initial conditions.

Here, the edge shearless curve ensemble is highlighted, demonstrating that within the same ensemble, orbits can belong to different coherent regions in phase space depending on their initial location. Consequently, the way ensembles are prepared, iterating one single orbit in the frozen system ($\phi = \text{const.}$), may not provide a good representation of populations of orbits with similar time evolution.

In fact, the dynamics of the frozen system bear little resemblance to those of the parameter-drift system. Consequently, one may expect that this ensemble definition leads to distinct properties, as reflected in the distribution of FTLEs and the structure of Lagrangian Coherent Structures within the ensemble.

Furthermore, the method employed here allows the computation of the full Lyapunov spectrum, not just the largest exponent. In our case, involving a two-dimensional parameter-drift Hamiltonian map, the system has only two Lyapunov exponents, which are additive inverses of each other, $(\lambda, -\lambda)$. Thus, the second exponent serves as a benchmark for verifying the reliability and accuracy of the computed largest FTLE. The primary advantage of this method, however, becomes evident in higher-dimensional systems. While the ensemble-average method yields only the largest Lyapunov exponent, the Jacobian-based approach enables a more comprehensive characterization of the orbit by providing the entire Lyapunov spectrum.

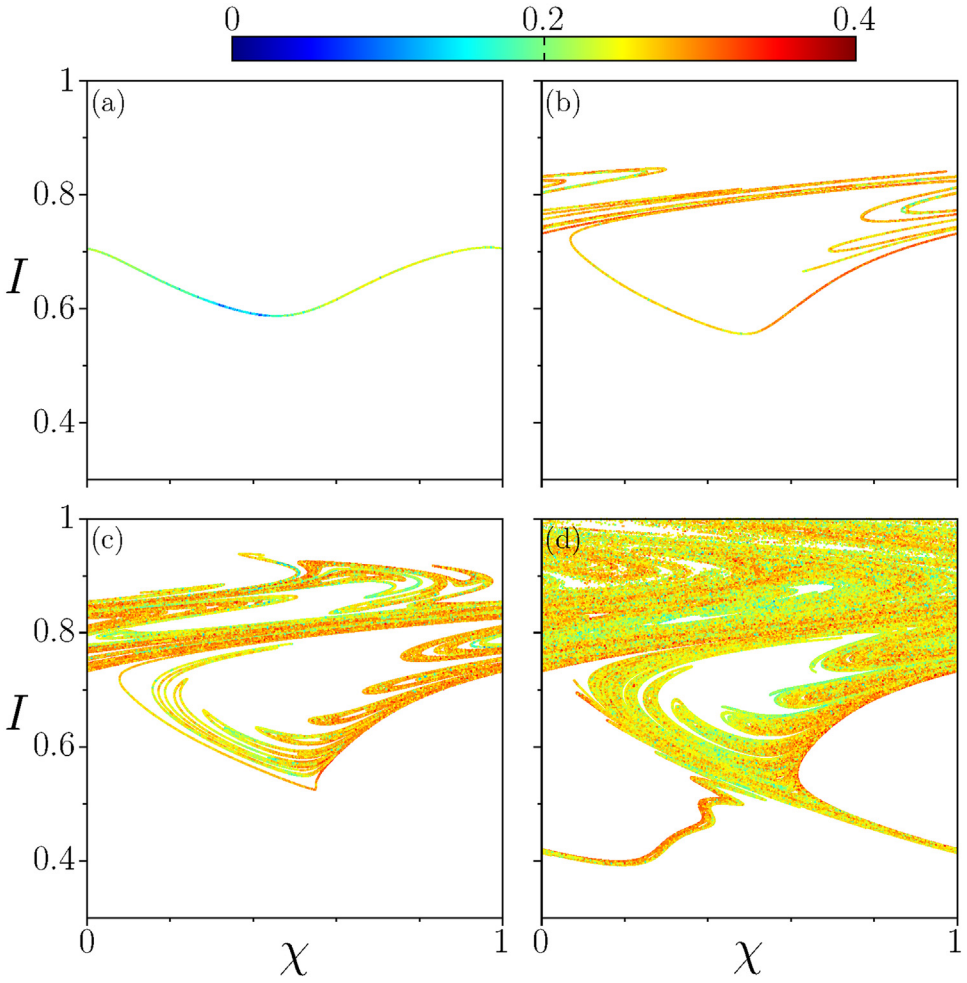

FIG. 5. Snapshots of the blue ensemble in Fig. 3 after n iterations. Colors represent the maximum finite-time Lyapunov exponent after (a) $n = 40$, (b) $n = 60$, (c) $n = 65$, and (d) $n = 75$ iterations.

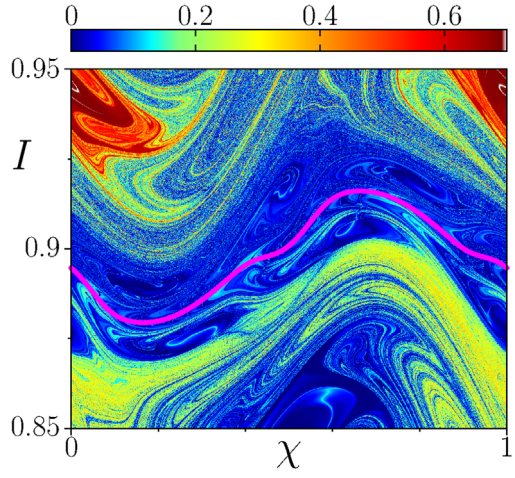

FIG. 6. Finite-time Lyapunov exponent after $n = 30$ iterations in (χ, I) plane of initial conditions. Parameters are $\phi_0 = 1.0 \times 10^{-3}$, $\phi' = 3 \times 10^{-5}$. Magenta points highlight the edge of the shearless orbit.

V. CONCLUSIONS

In the past decade, parameter-drift systems have been extensively studied in the context of low-dimensional dynamical systems, revealing insightful behaviors. Only recently have these models been applied to simplified physical systems, such as those in plasma physics, where they are showing promising results. The parameter-drift approach enables the inclusion of evolving parameters within the system dynamics without the computational cost of fully self-consistent simulations—a key advantage for modeling time-dependent scenarios in plasma discharges.

Traditionally, the ensemble approach has dominated studies of parameter-drift systems, particularly in dissipative settings where attractors are well-defined. In such cases, the specific choice of initial conditions does not affect the asymptotic behavior, and ensemble averages provide reliable information. However, for Hamiltonian systems or transient regimes lacking invariant limiting sets, the ensemble approach exhibits important limitations. Notably, the choice of initial ensemble is no longer unique, and ensemble-averaged quantities yield only typical, not representative, characterizations of the system dynamics. As shown in this tutorial through finite-time Lyapunov exponent

(FTLE) analysis, distinct subpopulations within an ensemble can exhibit considerably different transient behaviors. Moreover, the conventional method of preparing ensembles, using orbits evolved in the frozen (non-drifting) system, results in inhomogeneous distributions that do not follow the Lagrangian Coherent Structures of the true parameter-drift system.

To address these challenges, an alternative approach involves tracking individual orbits and analyzing their dynamical indicators independently. This orbit-wise strategy avoids the ambiguity inherent in ensemble definitions and highlights the diversity of transient behaviors. However, the explicit time dependence of parameter-drift systems poses a technical obstacle. To overcome this, we presented a method to embed the time-dependent system into an extended phase space, providing a time-independent character and preserving the Hamiltonian structure. This framework allows the application of standard tools for Lyapunov spectrum computation and, as we showed, provides a more accurate and detailed picture of the dynamics in parameter-drift Hamiltonian systems.

In such a higher-dimensional phase space, the Arnold web and associated Arnold diffusion provide natural mechanisms for global transport along resonance networks. In such settings, slow parameter variation causes orbits to migrate along these resonant pathways, producing long-range transport similar in spirit to Arnold diffusion. Exploring how parameter drift modifies the connectivity of the Arnold web is therefore a promising direction for future work, especially for applications involving multidimensional guiding-center models.

Although developed here in the context of drift-wave transport, the techniques presented may be applied more broadly to other relevant systems with slow or prescribed parameter evolution, such as transport phenomena and quasi-static evolution scenarios in magnetohydrodynamics.

Obviously, self-consistent models in plasma physics are more physically consistent compared to parameter-drift models due to their nature. However, the computational cost of fully self-consistent models is prohibitive in certain simulations, and the accuracy of both approaches depends intrinsically on the quality of the model and how coupled to other variables a given parameter is.

We hope this tutorial and the tools presented here assist the plasma physics community in recognizing the relevance of parameter-drift models, as well as in understanding their advantages and the limitations that remain to be addressed.

ACKNOWLEDGMENTS

P.J.M. was supported by U.S. Department of Energy Grant No. DE-FG02-04ER54742. This research was also supported by the National Council for Scientific and Technological Development (CNPq), Brazil, under Grant No. 302665/2017-0, and the São Paulo Research Foundation (FAPESP), Brazil, under Grants Nos. 2024/05700-5, 2022/05667-2, and 2024/02591-0.

AUTHOR DECLARATIONS

Conflict of Interest

The authors have no conflicts to disclose.

Author Contributions

Gabriel C. Grime: Data curation (equal); Formal analysis (equal); Investigation (lead); Methodology (equal); Validation (equal); Visualization (lead); Writing – original draft (lead); Writing – review & editing (equal). **Iberê L. Caldas:** Conceptualization (supporting); Funding acquisition (lead); Project administration (supporting); Supervision (equal); Validation (equal); Writing – review & editing (equal). **Philip J. Morrison:** Conceptualization (lead); Formal analysis (supporting); Methodology (equal); Project administration (equal); Resources (lead); Supervision (equal); Validation (equal); Writing – original draft (supporting); Writing – review & editing (equal).

DATA AVAILABILITY

The data that support the findings of this study are available from the corresponding author upon reasonable request.

REFERENCES

[1]T. Tajima, *Computational Plasma Physics: With Applications to Fusion and Astrophysics* (CRC Press, 2018).
[2]W. M. Tang and V. S. Chan, "Advances and challenges in computational plasma science," Plasma Phys. Controlled Fusion **47**, R1 (2005).
[3]J. Shalf, "The future of computing beyond Moore's Law," Philos. Trans. R. Soc. A **378**, 20190061 (2020).
[4]E. P. Alves and F. Fiuza, "Data-driven discovery of reduced plasma physics models from fully kinetic simulations," Phys. Rev. Res. **4**, 033192 (2022).
[5]I. Abramovic, E. Alves, and M. Greenwald, "Data-driven model discovery for plasma turbulence modelling," J. Plasma Phys. **88**, 895880604 (2022).
[6]D. Jánosi and T. Tél, "Overview of the advances in understanding chaos in low-dimensional dynamical systems subjected to parameter drift: Parallel dynamical evolutions and "climate change" in simple systems," Phys. Rep. **1092**, 1–64 (2024).
[7]E. L. Rempel, A. C.-L. Chian, S. de S. A. Silva, V. Fedun, G. Verth, R. A. Miranda, and M. Gošić, "Lagrangian coherent structures in space plasmas," Rev. Mod. Plasma Phys. **7**, 32 (2023).
[8]K. Bai, D. Ji, and E. Brown, "Ability of a low-dimensional model to predict geometry-dependent dynamics of large-scale coherent structures in turbulence," Phys. Rev. E **93**, 023117 (2016).
[9]P. J. Holmes, J. L. Lumley, G. Berkooz, J. C. Mattingly, and R. W. Wittenberg, "Low-dimensional models of coherent structures in turbulence," Phys. Rep. **287**, 337–384 (1997).
[10]D. del Castillo-Negrete and P. J. Morrison, "Chaotic transport by Rossby waves in shear flow," Phys. Fluids A **5**, 948–965 (1993).
[11]P. J. Morrison, "Magnetic field lines, Hamiltonian dynamics, and nontwist systems," Phys. Plasmas **7**, 2279–2289 (2000).
[12]M. Farazmand, D. Blazevski, and G. Haller, "Shearless transport barriers in unsteady two-dimensional flows and maps," Physica D **278–279**, 44–57 (2014).
[13]*Magnetic Stochasticity in Magnetically Confined Fusion Plasmas: Chaos of Field Lines and Charged Particle Dynamics*, Springer Series on Atomic, Optical, and Plasma Physics Vol. 78, edited by S. Abdullaev (Springer, 2014).
[14]M.-C. Firpo and D. Constantinescu, "Study of the interplay between magnetic shear and resonances using Hamiltonian models for the magnetic field lines," Phys. Plasmas **18**, 032506 (2011).
[15]A. H. Boozer, "Plasma equilibrium with rational magnetic surfaces," Technical Report No. PPPL-1762 (Princeton Plasma Physics Lab. (PPPL), Princeton, NJ, 1981).
[16]F. A. Marcus, I. L. Caldas, Z. d. O. Guimarães-Filho, P. J. Morrison, W. Horton, Y. K. Kuznetsov, and I. C. Nascimento, "Reduction of chaotic particle transport driven by drift waves in sheared flows," Phys. Plasmas **15**, 112304 (2008).
[17]J. R. Cary and A. J. Brizard, "Hamiltonian theory of guiding-center motion," Rev. Mod. Phys. **81**, 693–738 (2009).
[18]R. B. White and M. S. Chance, "Hamiltonian guiding center drift orbit calculation for toroidal plasmas of arbitrary cross section," Technical Report No. PPPL-2089 (Princeton Plasma Physics Lab. (PPPL), Princeton, NJ, 1984).
[19]W. Horton, H.-B. Park, J.-M. Kwon, D. Strozzi, P. J. Morrison, and D.-I. Choi, "Drift wave test particle transport in reversed shear profile," Phys. Plasmas **5**, 3910 (1998).
[20]W. W. Heidbrink and R. B. White, "Mechanisms of energetic-particle transport in magnetically confined plasmas," Phys. Plasmas **27**, 030901 (2020).

[21]G. Anastassiou, P. Zestanakis, Y. Antonenas, E. Viezzer, and Y. Kominis, "Role of the edge electric field in the resonant mode-particle interactions and the formation of transport barriers in toroidal plasmas," J. Plasma Phys. **90**, 905900110 (2024).
[22]M. Ghil and D. Sciamarella, "Dynamical systems, algebraic topology and the climate sciences," Nonlinear Processes Geophys. **30**, 399–434 (2023).
[23]J. H. Li, F. X.-F. Ye, H. Qian, and S. Huang, "Time-dependent saddle–node bifurcation: Breaking time and the point of no return in a non-autonomous model of critical transitions," Physica D **395**, 7–14 (2019).
[24]T. Tél, T. Bódai, G. Drótos, T. Haszpra, M. Herein, B. Kaszás, and M. Vincze, "The theory of parallel climate realizations: A new framework of ensemble methods in a changing climate: An overview," J. Stat. Phys. **179**, 1496–1530 (2020).
[25]C. Leith, "Predictability of climate," Nature **276**, 352–355 (1978).
[26]D. Jánosi and T. Tél, "Chaos in Hamiltonian systems subjected to parameter drift," Chaos **29**, 121105 (2019).
[27]D. Jánosi, A. Horváth, L. Édes, and T. Kovács, "Magnetic structures in the explicitly time-dependent nontwist map," Chaos **34**, 123160 (2024).
[28]E. Illés, D. Jánosi, and T. Kovács, "Orbital dynamics in galactic potentials under mass transfer," Astron. Astrophys. **692**, A240 (2024).
[29]D. Jánosi and T. Tél, "Characterizing chaos in systems subjected to parameter drift," Phys. Rev. E **105**, L062202 (2022).
[30]A. J. Lichtenberg and M. A. Lieberman, *Regular and Chaotic Dynamics* (Springer Science & Business Media, 2013), Vol. 38.
[31]S. S. Abdullaev, *Construction of Mappings for Hamiltonian Systems and Their Applications* (Springer, 2006), Vol. 691.
[32]D. del-Castillo-Negrete and P. J. Morrison, "Hamiltonian chaos and transport in quasigeostrophic flows," in *Chaotic Dynamics and Transport in Fluids and Plasmas*, Research Trends in Physics, edited by I. Prigogine (American Institute of Physics, New York, NY, 1993), pp. 181–207.
[33]D. del Castillo-Negrete and P. J. Morrison, "Magnetic field line stochasticity and reconnection in a non-monotonic q-profile," Bull. Am. Phys. Soc. Ser. II **37**, 1543 (1992).
[34]D. del Castillo-Negrete, J. M. Greene, and P. J. Morrison, "Area preserving nontwist maps: Periodic orbits and transition to chaos," Physica D **91**, 1 (1996).
[35]D. del Castillo-Negrete, J. M. Greene, and P. J. Morrison, "Renormalization and transition to chaos in area preserving nontwist maps," Physica D **100**, 311–329 (1997).
[36]W. Horton, P. J. Morrison, X. R. Fu, and J. Pratt, "Transport with reversed E_r in the Gamma-10 tandem mirror," Trans. Fusion Sci. Technol. **55**, 15–18 (2009).
[37]C. W. Horton, *Turbulent Transport in Magnetized Plasmas* (World Scientific, 2012).
[38]J. W. Connor, T. Fukuda, X. Garbet, C. Gormezano, V. Mukhovatov, M. Wakatani *et al.*, "A review of internal transport barrier physics for steady-state operation of tokamaks," Nucl. Fusion **44**, R1 (2004).
[39]E. Viezzer, T. Pütterich, G. D. Conway, R. Dux, T. Happel, J. C. Fuchs, R. M. McDermott, F. Ryter, B. Sieglin, W. Suttrop *et al.*, "High-accuracy characterization of the edge radial electric field at ASDEX upgrade," Nucl. Fusion **53**, 053005 (2013).
[40]G. G. Grenfell, I. Nascimento, D. Oliveira, Z. Guimarães-Filho, J. Elizondo, A. Reis, R. M. O. Galvão, W. A. H. Baquero, A. M. Oliveira, G. Ronchi *et al.*, "H-mode access and the role of spectral shift with electrode biasing in the TCABR tokamak," Phys. Plasmas **25**, 072301 (2018).
[41]R. M. O. Galvão, C. H. S. Amador, W. A. H. Baquero, F. Borges, I. L. Caldas, N. A. M. Cuevas, V. N. Duarte, A. G. Elfimov, J. Elizondo, A. M. M. Fonseca *et al.*, "Report on recent results obtained in TCABR," J. Phys.: Conf. Ser. **591**, 012001 (2015).
[42]J. D. Szezech, I. L. Caldas, S. R. Lopes, R. L. Viana, and P. J. Morrison, "Transport properties in nontwist area-preserving maps," Chaos **19**, 043108 (2009).
[43]E. A. Coddington and N. Levinson, *Theory of Ordinary Differential Equations* (McGraw-Hill Book Co., 1955).
[44]C. Kuehn, "A mathematical framework for critical transitions: Bifurcations, fast–slow systems and stochastic dynamics," Physica D **240**, 1020 (2011).
[45]N. Berglund and B. Gentz, *Noise-Induced Phenomena in Slow-Fast Dynamical Systems* (Springer, London, 2006).
[46]D. Jánosi, G. Károlyi, and T. Tél, "Climate change in mechanical systems: The snapshot view of parallel dynamical evolutions," Nonlinear Dyn. **106**, 2781–2805 (2021).
[47]G. Montani, M. Del Prete, N. Carlevaro, and F. Cianfrani, "Diffusive time evolution of the Grad–Shafranov equation for a toroidal plasma," J. Plasma Phys. **87**, 845870301 (2021).
[48]C. Hansen, I. G. Stewart, D. Burgess, M. Pharr, S. Guizzo, F. Logak, A. O. Nelson, and C. Paz-Soldan, "TokaMaker: An open-source time-dependent Grad-Shafranov tool for the design and modeling of axisymmetric fusion devices," Comput. Phys. Commun. **298**, 109111 (2024).
[49]M. V. de Moraes, I. L. Caldas, and Y. Elskens, "Non-autonomous standard nontwist map," Chaos, Solitons Fractals **198**, 116492 (2025).
[50]J. D. Meiss, "Thirty years of turnstiles and transport," Chaos **25**, 097602 (2015).
[51]G. C. Grime, I. L. Caldas, R. L. Viana, and Y. Elskens, "Effective transport barriers in the biquadratic nontwist map," Phys. Rev. E **111**, 014219 (2025).
[52]D. Jánosi and T. Tél, "Chaos in conservative discrete-time systems subjected to parameter drift," Chaos **31**, 033142 (2021).
[53]P. J. Morrison, "Hamiltonian description of the ideal fluid," Rev. Mod. Phys. **70**, 467–521 (1998).
[54]J. L. Safko, H. Goldstein, and C. Poole, *Classical Mechanics* (Pearson Education, Inc, 2002).
[55]V. I. Arnol'd, *Mathematical Methods of Classical Mechanics* (Springer Science & Business Media, 2013), Vol. 60.
[56]G. C. Grime and P. J. Morrison, "Construction of symplectic systems from parameter-drift Hamiltonian maps," arXiv:2505.04750 (2025).
[57]B. V. Chirikov, "A universal instability of many-dimensional oscillator systems," Phys. Rep. **52**, 263–379 (1979).
[58]V. I. Arnold, "Instability of dynamical systems with several degrees of freedom," in *Collected Works: Representations of Functions, Celestial Mechanics and KAM Theory, 1957–1965*, edited by A. B. Givental *et al.* (Springer, Berlin Heidelberg, 2009), pp. 423–427.
[59]C.-Q. Cheng and J. Xue, "Some recent developments in Arnold diffusion," in *Hamiltonian Systems: Dynamics, Analysis, Applications*, Mathematical Sciences Research Institute Publications (Cambridge University Press, 2024), pp. 75–110.
[60]A. Delshams, R. de la Llave, and T. M. Seara, *A Geometric Mechanism for Diffusion in Hamiltonian Systems Overcoming the Large Gap Problem: Heuristics and Rigorous Verification on a Model* (American Mathematical Society, 2006), Vol. 179.
[61]A. Delshams, R. de la Llave, and T. M. Seara, "Geometric properties of the scattering map of a normally hyperbolic invariant manifold," Adv. Math. **217**, 1096–1153 (2008).
[62]P. Bernard, V. Kaloshin, and K. Zhang, "Arnold diffusion in arbitrary degrees of freedom and normally hyperbolic invariant cylinders," Acta Math. **217**, 1–79 (2016).
[63]M. Gidea and J.-P. Marco, "Diffusing orbits along chains of cylinders," Discrete Contin. Dyn. Syst. **42**, 5737–5782 (2022).
[64]A. Luque and D. Peralta-Salas, "Arnold diffusion of charged particles in ABC magnetic fields," J. Nonlinear Sci. **27**, 721–774 (2017).
[65]A. H. Boozer, "Arnold diffusion and adiabatic invariants," Phys. Lett. A **185**, 423–427 (1994).
[66]A. Wolf, J. B. Swift, H. L. Swinney, and J. A. Vastano, "Determining Lyapunov exponents from a time series," Physica D **16**, 285–317 (1985).
[67]G. Haller and G. Yuan, "Lagrangian coherent structures and mixing in two-dimensional turbulence," Physica D **147**, 352–370 (2000).
[68]F. Lekien, S. C. Shadden, and J. E. Marsden, "Lagrangian coherent structures in n-dimensional systems," J. Math. Phys. **48**, 065404 (2007).
[69]G. Haller, "Lagrangian coherent structures," Annu. Rev. Fluid Mech. **47**, 137–162 (2015).